Nanoscale

Surfactant-mediated Morphology Evolution and Self-assembly of Cerium Oxides Nanocrystals for Catalytic and Supercapacitor Applications

Journal:	*Nanoscale*
Manuscript ID	NR-ART-03-2021-001746.R1
Article Type:	Paper
Date Submitted by the Author:	03-May-2021

Complete List of Authors:	Hao, Xiaodong; Shaanxi University of Science and Technology, Materials Institute of Atomic and Molecular Science Zhang, Shuai; Shaanxi University of Science and Technology, Materials Institute of Atomic and Molecular Science Xu, Yang; Shaanxi University of Science and Technology, Materials Institute of Atomic and Molecular Science Tang, Liangyu; Tohoku University, WPI-Advanced Institute for Materials Research Inoue, Kazutoshi ; Tohoku University, WPI-Advanced Institute for Materials Research Saito, Mitsuhiro ; The University of Tokyo, Institute of Engineering Innovation Ma, Shufang; Shaanxi University of Science and Technology, Materials Institute of Atomic and Molecular Science Chen, Chunlin; Institute of Metal Research Chinese Academy of Sciences, Shenyang National Laboratory for Materials Science Xu, Bingshe; Shaanxi University of Science and Technology, Materials Institute of Atomic and Molecular Science Adschiri, Tadafumi; Tohoku University, WPI-Advanced Institute for Materials Research Ikuhara, Yuichi; The University of Tokyo, Institute of Engineering Innovation, School of Engineering; Tohoku University, WPI-Advanced Institute for Materials Research

Article

Surfactant-mediated Morphology Evolution and Self-assembly of Cerium Oxides Nanocrystals for Catalytic and Supercapacitor Applications

Received 00th January 20xx,
Accepted 00th January 20xx

DOI: 10.1039/x0xx00000x

Xiaodong Hao,*[a,b] Shuai Zhang,[a,c] Yang Xu,[a,c] Liangyu Tang,[b] Kazutoshi Inoue[b], Mitsuhiro Saito[d], Shufang Ma[a], Chunlin Chen[e], Bingshe Xu*[a], Tadafumi Adschiri*[b] and Yuichi Ikuhara*[b,d]

Surfactant plays a remarkable role in determining the growth process (facet exposition) of colloidal nanocrystals (NCs) and the formation of self-assembled NCs superstructures, which, however, still requires proofs for elucidating the underlying mechanism. Here, this work elucidates the mechanism of surfactant-mediated morphology evolution and self-assembly of CeO_2 nanocrystals by exploring the effect of surfactant modification on the shapes, size, exposing facets, and arrangement of CeO_2 NCs. It directly proves that surfactant molecule determines the morphologies of CeO_2 NCs by preferentially bonding onto the Ce-terminated {100} facets, changing from large truncated octahedron (mostly exposing {111} and {100}), to cube (mostly exposing {100}) and small cuboctahedron (mostly exposing {100} and {111}) by increasing the amount of surfactant. The exposure degree of {100} facets largely affects the concentration of Ce^{3+} in CeO_2 NCs, thus the cubic CeO_2 NCs exhibits a superior oxygen storage capacity and an excellent supercapacitor performance owing to the high exposure fraction of active {100} facets with great superstructure stability.

Ever since the terminology of nanocrystals (NCs) appeared three decades ago, continuous interest has been paid to the synthesis and characterization strategies, aiming to unravel its intrinsic features over bulk materials and bring prospective insights into the practical application of NCs.[1-2] A variety of colloidal NCs systems has been fabricated with controllable morphologies, sizes, and compositions, and held substantial potential in the fields of environmentally friendly catalysts, energy storage materials, and biological applications.[3-6] It is reported that NCs could also be encapsulated into the organic coordination cages to work synergistically with the restricted cavity for improved performance.[7-9] In addition, owing to the remarkable chemical synthesis methods, the large-scale fabrication of monodispersed colloidal NCs become possible, and they are readily order into complex structures via self-assemble method.[10-11] Colloidal NCs superlattice, firstly reported in 1995[12] and later praised as a low-tech route to a potentially high-tech material, has opened up a whole new world of versatile superstructures, including semiconductor quantum dots,[13] metal and metal oxides nanoparticles,[10, 14] and binary nanocrystals.[15-16] In addition to the fundamental role of individual nanoparticles, the structural hierarchy and compositional tunability of colloidal NCs superlattices equip these materials with novel electronic, optical, mechanical, and catalytic functionality for nano-technological applications.[17-18] For both colloidal NC itself and the ordered NCs superstructure, the surface chemistry is essential and requires much attentions.[19-20]

In shaping the morphologies of colloidal NCs, surfactant ligand plays a key role in determining the growth and stability of NCs by chemically bonding onto the preferential facets.[21] By adjusting the surfactant addition into the chemical reaction system, it is feasible to control the morphologies of NCs with desired exposing facets.[22] Furthermore, the technical improvement in the field of materials characterization is capable of the direct observation of the surfactant coverage on NCs via various approaches,[23] particularly by small-angel X-ray scattering,[24] scanning tunneling microscopy,[25] high resolution transmission electron microscopy (TEM),[26] and even the direct imaging of molecular chain of surfactant by aberration corrected scanning transmission electron microscopy (STEM).[27] Meanwhile, the in-situ TEM techniques make it possible to directly observe the surfactant-assisted growth of metal NCs in a liquid cell,[28] and kinetically-driven shape transformation in an etching solution.[29] Advances in specialized knowledge and technology of the NCs synthesis and characterization aim at unravelling the internal mechanisms of NCs formation and facet evolution, to fabricate NCs in atomically precision in the near future.[30]

Cerium dioxide (CeO_2) has been recognized as the promising candidates for catalysts and solid electrolytes owing to its high oxygen storage capacity (OSC) and high oxygen mobility.[31-35] Effective chemical solutions have been developed for the fabrication of CeO_2 NCs with tailored morphology, narrow size distribution, active dopants and exposing facets.[27, 36-39] It has been reported that the catalytic reactivity of CeO_2 NCs are usually dependent on their shapes, particularly the exposing facets.[40-42] Therefore, the control over the shapes of CeO_2 NCs is essential to adjust its properties so as to be suitable for a given application. In this work, we systematically explored the morphology evolution of CeO_2 NCs by fine-tuning the addition of surfactant ligand in supercritical water. Supercritical

[a] *Materials Institute of Atomic and Molecular Science, Shaanxi University of Science and Technology, Xi'an 710021, China. E-mail: hao.xiaodong@sust.edu.cn; xubingshe@sust.edu.cn*
[b] *WPI-Advanced Institute for Materials Research, Tohoku University, Sendai 980-8577, Japan. E-mail: tadafumi.ajiri.b1@tohoku.ac.jp*
[c] *School of Materials Science and Engineering, Shaanxi University of Science & Technology, Xi'an 710021, China*
[d] *Institute of Engineering Innovation, the University of Tokyo, Tokyo 116-0013, Japan. E-mail: ikuhara@sigma.t.u-tokyo.ac.jp*
[e] *Shenyang National Laboratory for Materials Science, Institute of Metal Research, Chinese Academy of Science Liaoning, 110016, China*
Electronic Supplementary Information (ESI) available: [XRD spectra, SAED patterns, FT-IR spectra, STEM-EELS mapping spectra, HAADF-STEM images, comparison of OSC and supercapacitor performance. See DOI: 10.1039/x0xx00000x

hydrothermal synthesis which uses water as a solvent and enables easy heat recovery is recognized as an environmentally benign method to synthesize colloidal NCs. It was found that the increased amount of surfactant ligand had a significant effect on the morphology, size and distribution of CeO_2 NCs. In particular, the shape of NCs changed from large truncated octahedra (in the size of over 10 nm), to cubic (approximately 5 nm), and small cuboctahedra (approximately 4 nm), along with the increasing of surfactant ligand. The self-assembly of the cubic CeO_2 NCs into monolayer NCs superstructure was also revealed. Moreover, the catalytic and supercapacitor performance of representative samples of surfactant modified CeO_2 NCs were evaluated, showing a high OSC performance and specific capacitance for the cubic CeO_2 NCs, which was attributed to the exposure of highly reactive facets of {100} and smaller NCs size. Overall, these results pave the basis for understanding the surfactants influencing on nanocrystals morphology and provide strategies for forming well-engineered nanocrystals.

Surfactant-mediated Shape Evolution of CeO_2 NCs. The fabrication of metal oxides NCs possessing with morphology, narrow size distribution, and active exposing facets attracts the extensive attention in the field of nanomaterials and surface chemistry. Among all the chemical approaches, supercritical water for nanoparticle synthesis has been showing a superior ability for aiding the spontaneous nucleation and controlled growth process because of the unique medium. In addition, separation/concentration of NCs is of energy consuming process, but in this supercritical method, organic modified NCs can be recovered (extracted) automatically to an organic phase after the phase separation (organic phase–water phase) by decreasing temperature at the exit of the reactor. This significantly reduces the energy consumption, which is another aspect of green chemistry process of this method. In comparison with commonly used two-phase hydrothermal reaction under the moderate temperature (100-200°C), the organic surfactant is miscible with the inorganic metal oxides precursor solution in supercritical condition, leading to the in-situ surface modification of nanocrystal during the growth process.[27, 37] By fine-tuning the addition amount of the organic surfactant, the morphologies, size, exposed facets, and the distribution of as-synthesized NCs can be adjusted properly. In detail, a batch of CeO_2 NCs were synthesized by changing the molar ratio of surfactant to Ce with *n:1* (*n=0, 1, 2, 5, 6, 8, 15, and 30*) in the supercritical reaction. Here, the samples are marked as Sm-CeONC-n where *Sm*, *CeONC*, and *n* represent surfactant modified, CeO_2 NCs and the molar ratio of surfactant to Ce, respectively. The crystal structure of the as-synthesized Sm-CeONCs was examined by means of powder X-ray diffraction (XRD), indicating four strong diffraction peaks of 111, 200, 220, 311, which were indexed to the fluorite-cubic structure of CeO_2 (see Supporting Information, Figure S1).

In addition, the morphologies of the Sm-CeONCs were systematically observed using TEM and STEM imaging and electron diffraction techniques, as shown in Figure 1 and S3. Without the surfactant modification (Sm-CeONC-0), the NCs tends to be the octahedra shapes with a great extent of aggregation (Figure 1A). For CeO_2, {111} facets present the lowest surface energy and stable surface structure compared to {110} and {100}, so that {111} facets are mostly exposed outside.[33] Thus, the {111} diffraction appears in dominate intensity in the selective area electron diffraction (SAED) pattern when the electron beam diffract with the NCs that are randomly deposited on the flat substrate (Figure S3A). By a low amount of surfactant ligand to the reaction system, the sample of Sm-CeONCs-1 presents mostly in the shape of truncated octahedra (Figure 1B), in which {100} facets form in some extent because of the surfactant modification. Gradually, it changes to the cubic-like morphology in the case of Sm-CeONC-2, while the NCs aggregation still exists since the surfactant merely attaches onto the {100} facets (Figure 1C). Actually, the morphologies undergo the quick transformation at the initial addition of surfactant from Sm-CeONC-0 to Sm-CeONC-2, thus the magnified STEM images are also recorded for clearly showing the shape change as shown in Figure S2. Along with the increased addition of surfactant ligand, the growth along <001> orientation is largely limited by the surfactant attachment, so that {100} facets become dominate exposing facets and monodispersed cubic CeO_2 NCs are mostly formed and well-distributed on the substrate (Figure 1D-G). Such kind of cubic NCs favors the arrangement of {100} face-up monolayer superstructure after the deposition on the ultrathin and flat carbon substrate, because of which the intensity of {200} diffraction ring is firstly increased to an equivalent level as {111} ring and subsequent became dominant; whereas, the {111} ring is gradually reduced when the electron beam diffraction occurs along the <001> direction (Figure S3B-G). Further increase of the surfactant addition gives rise to the formation of the small cuboctahedra CeO_2 NCs in a certain amount owing to the fact that superfluous surfactant addition inhibits the growth process in a large extent (Figure 1H-I). Therefore, these smaller NCs in cuboctahedra shape hardly arranges as the {100} face-up arrangement so that {111} diffraction appears again and increases up to the equivalent level of intensity to the {200} diffraction in Sm-CeONC-30 (Figure S3H-I). Comparatively, the size of NCs is affected by the surfactant modification, which was both confirmed by the analysis of TEM images and XRD spectra as illustrated in Figure S4. It changes from above 10 nm for Sm-CeONC-0, to approximately 6 nm when introducing a certain amount of surfactant (up to Sm-CeONC-6), and it subsequently decreases to a smaller size of approximately 5 nm with further addition of surfactant from Sm-CeONC-8 to Sm-CeONC-30. Therefore, these results clearly elaborate the surfactant-assisted process of morphologies evolution of NCs in supercritical water, i.e. the transformation of {100} facet along with the surfactant modification. Therefore, the preferable shapes with desired exposing facets could be achieved by fine-tuning the surfactant modification to the reaction process.

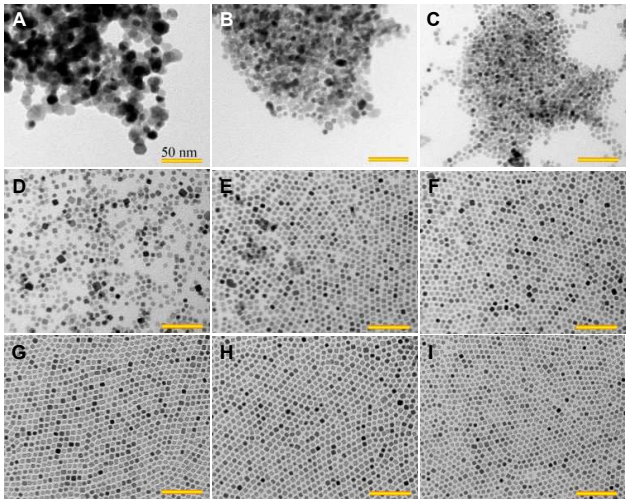

Figure 1. Microstructure analysis of surfactant modified CeO_2 NCs. TEM images of as-synthesized CeO_2 NCs under different addition of surfactant molecules: A) Sm-CeONC-0, B) Sm-CeONC-1, C) Sm-CeONC-2, D) Sm-CeONC-

3, E) Sm-CeONC-5, F) Sm-CeONC-6, G) Sm-CeONC-8, H) Sm-CeONC-15, I) Sm-CeONC-30. The scale bar is 50 nm.

Direct Determination of Surfactant Coverage on CeO_2 NCs. Given that the substantial influence of surfactant modification on the morphologies and size of NCs, the investigation of surfacant coverage becomes essential. To understand the interaction between the NCs and the organic molecules, the Fourier transform infrared spectroscopy (FT-IR) of the Sm-CeONC were obtained and analysed (see details in Figure S5). The FT-IR spectra indicate the chelating bidentate bonding nature of two oxygen atoms of the carboxylate group from surfactant molecules onto a cerium cation for all the test samples of Sm-CeONCs.[43] In order to understand this issue clearly, the atomic-resolution STEM images and electron energy loss spectroscopy (EELS) mappings of the representative samples of Sm-CeONCs were provided in Figure 2 and Figure S6. Figure 2B shows that Sm-CeONC-1 exposes mainly in {111} and a relatively smaller fraction of {100} facets. The EELS mapping spectrum shows the elemental distribution of C *K* edge (in red), Ce *M* edge (in green), and O *K* edge (in red), in which the C *K* edge indicates the distribution of surfactant molecules as presented in our previous report.[27] Figure S6A indicates that the surfactant coverage of Sm-CeONC-1 is low and the NCs tend to be attached and disorderly aggregated . When increasing the surfactant amount to the condition of Sm-CeONC-6, the NCs compose of mostly {100} facets exposure, and a little fraction of {111} edge, as illustrated in Figure 2C. Afterwards, it changes to monodispersed cubic NCs and the distinct and clear distribution of surfactant coverage is observed in Figure S6B. Moreover, Figure 2E-H displays the atomic resolution EELS mapping spectra of a single cubic NC. It clearly shows a slight decrease of surfactant density at the edges and corners pointed out by the white arrows on the C *K* spectrum compared to the main {100} facets, indicating of a low surfactant coverage. Further increase of the surfactant modification would inhibit the NCs growth by fully covering the NCs from all direction as indicated by the EELS mapping in Figure S6C. Thus, the shape of Sm-CeONC-30 transform from the cube to cuboctahedron that the exposure of {111} facets is increased as shown in Figure 2D. In addition, the crystal models concerning the exposing facets and size are built to estimate the facets fraction of {111}, {110}, and {100} during the morphology transformation (as shown in Table S1). It shows that the Sm-CeONC-1 in the shape of truncated octahedron mainly exposes {111} facet with a high fraction of 88.43%, and a little fraction of 11.57% for the {100} facet. Whereas, the cubic shape is mainly composed of {100} facets 82.20%, and fraction of {111} is reduced to be 0.62%. Instead, {110} edge is formed and the fraction is reached up to 17.18%. For the cuboctahedron CeO_2 NCs, the {100} exposure is decreased to be 63.40% during to the formation of {111} facet in the faction of 33.6% because of the excessive amount of surfactant addition.

Based on these direct STEM-EELS mappings of surfactant distribution, the substantiation proofs for the proposed growth mechanism[37] is provides as illustrated in Figure 2A and the proposed crystal models of the distribution of surfactant molecules on CeO_2 NCs in Figure S6: (a) in the low surfactant amount (such as Sm-CeONC-1), the functional group of surfactant molecules preferentially interacts {100} facets so that the growth along <001> direction is limited, leading to the formation of large truncated octahedra NCs with a small fraction of {100} facets; (b) in the intermediate addition (from Sm-CeONC-3 to -15), the growth of the CeO_2 NC in the <001> direction is largely inhibited because of the surfactant coverage, while the growth of NC in the <011> and <111> direction continues, resulted into the formation of cubic NCs with a little fraction of {110} edges and {111} cut-off corners where surfactant molecules scarcely covered; (c) excessive surfactant addition (Sm-CeONC-30) could inhibit the growth rate from all the directions, so that small cuboctahedra NCs forms that {100} and {111} exposing facets are fully covered by surfactant molecules. Therefore, by means of the advanced approach for the synthesis of CeO_2 NCs with surfactant modification in supercritical water and the direct observation of the selective distribution of surfactant on the exposed facets by STEM-EELS mapping, the distinct evidence is provided for the surfactant-mediated mechanism of facet evolution of CeO_2 NCs, and the formation of cubic NCs in the appropriate condition of surfactant modification.

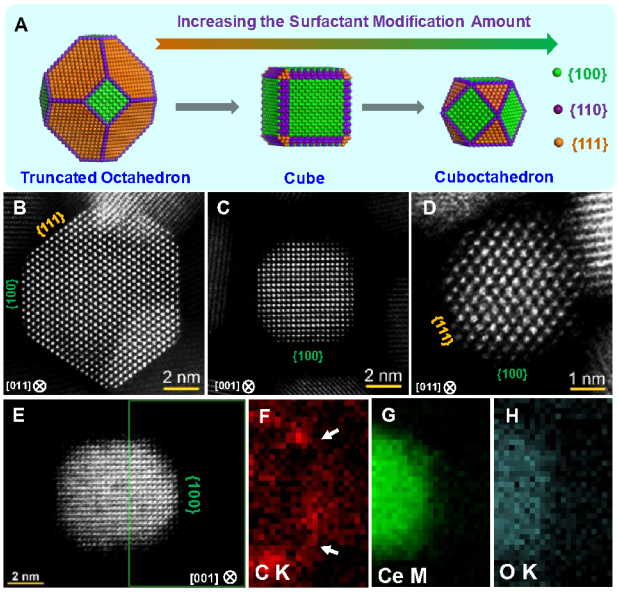

Figure 2. Direct determination of surfactant assistant facet evolution of CeO_2 NCs. (A) The crystal models of surfactant modified CeO_2 NCs in the shape of truncated octahedra, cubic and cuboctahedra, respectively. HAADF-STEM images of (B) Sm-CeONC-1, (C) Sm-CeONC-8, and (D) Sm-CeONC-30, respectively. Elemental mapping spectra of a single cubicCeO_2 NC: (E) raw ADF image, (F) carbon *K* edge, (G) cerium *M* edge, and (H) oxygen *K* edge, respectively. The NCs were deposited on silicon substrate for EELS mapping.

Surfactant-mediated Self-assembly of CeO_2 NCs Superstructure. In addition to facets evolution of CeO_2 NCs depending on the surfactant modification, the surfactant coverage plays an indispensable role on the arrangement of CeO_2 NCs that the relatively larger surfactant coverage results into well-distributed NCs superstructure, as can be seen in Figure 1F-I. The self-assembly process of NCs can also be fine-tuned by changing the deposition techniques, such as the concentration of NCs solution, deposition substrate, the deposition angle onto the substrate, drying rate, and so on.[18] The surfactant coverage affects the self-assembly of colloidal NCs to a well-distributed ordered superstructure when the balancing was achieved between the repulsive interactions by the surfactant molecules and the Van der Waals' attraction from the nearby NCs, or the capillary force occurred between the NCs during the drying process.[18, 44] Figure 3A-C shows the monolayer superstructure of {100}-faceted cubic NCs after depositing the one drop of colloidal Sm-CeONC-8 on a flat carbon substrate. The average interparticles spacing (*d*) was approximately 2 nm measured from the TEM image, indicating a surfactant mediated interpenetration interaction.[18, 27] The corresponding FFT in the inset of Figure 3A suggests a two dimensional NCs superlattice, in which the NCs may be regarded as the atoms and surfactant ligand as the bonds in the NCs

superlattice.[18, 45-46] Figure 3C indicates that the cubic NCs arranges mostly in {100} face to face configuration. In addition, the cubic CeO_2 NCs was further characterized by STEM imaging equipped with an annular bright field (ABF) and high angle annular dark field (HAADF) detectors. It is well-known that ABF image is able to resolve the light and heavy elements simultaneously, compared to the Z-contrast HAADF image that only heavy atoms are clearly seen.[47-48] It is clear that both Ce and O atoms are clearly observed in the ABF image in Figure 3D, while only Ce atoms are resolved in the HAADF image in Figure 3E, according to the atomic structure model atop the ABF image. Comparatively, it is confirmed that the cubic CeO_2 NCs are mostly {100}-faceted with Ce termination. The carboxylic group of the surfactant molecules are supposed to be boned onto the semi-coordinated Ce atoms of {100} facets, as interpreted from the FT-IR spectra in Figure S5. Whereas, the self-assembly of cuboctahedra CeO_2 NCs (Sm-CeONC-30) hardly holds the {100} face to face configuration because of increased exposure of {111} facets by excessive surfactant modification, and the arrangement is changed that from 4-coordinated to 6-coordinated, as shown in Figure S7. Meanwhile, multi-layer cubic NCs ordered superstructures are also achieved in the densely distributed regions, as displayed in Figure S8. It is suggested that the NCs in the top layer mostly locates atop the NCs corners (where surfactant density is low) from the bottom layer, resulted into the formation of the oriented arrangement of multi-layer cubic NCs superlattice.[49] Moreover, the thermal stability of cubic NCs superstructures was also tested in Figure S9. It shows that it could withstand a heat treatment of 200~500 °C without changing the original morphology and well-distributed arrangement, even at a high temperature of 500 °C for 1 hour. In this regard, surfactant-mediated cubic NCs superstructures, especially in three dimensional constructions, possessing high temperature thermal stability, could be readily efficiently in creating diverse metamaterials with complex compositions and structures.[50-51]

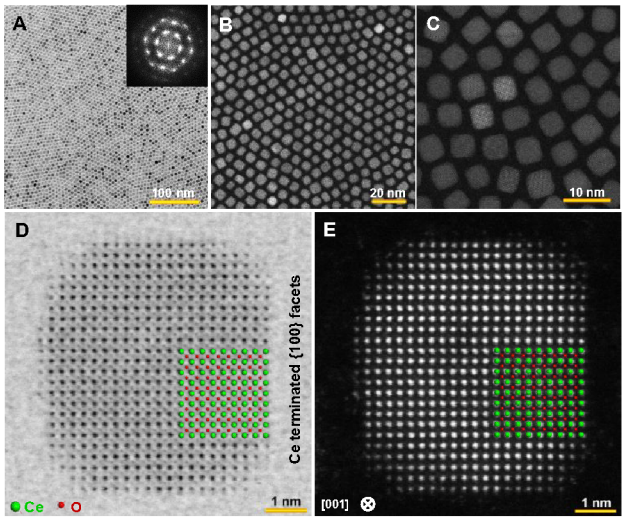

Figure 3. Self-assembly of cubic CeO_2 NCs. (A-C) Low magnification TEM and HAADF-STEM images of cubic CeO_2 NCs (Sm-CeONC-8) superstructure. (D, E) ABF- and HAADF images of a single cubic CeO_2 NC. The inset in (A) is the corresponding FFT pattern from the cubic CeO_2 NCs superstructure.

Shape-dependent of Cerium valence in Sm-CeONCs and its Catalytic Application and Supercapacitor Application. The surfactant attachment determines the shapes of the CeO_2 NCs by exposing different fraction of highly reduced {100} facets, which would infulence the valence state of cerium. In this regard, the Ce valence states were determined by measuring Ce *M* edge from the STEM-EELS spectra, as displayed in Figure 4A. As can be seen, there shows the featured peaks at around 886 V (M_5) and 905 eV (M_4), plotted by the two dot lines for the bulk CeO_2.[38-39, 52] It is clearly observed that peaks shift to the lower energy loss position for the sample of Sm-CeONC-8 and Sm-CeONC-30, comparing to the Sm-CeONC-1, indication of the transformation of cation valence from tetravalent (Ce^{4+}) to trivalent (Ce^{3+}). Moreover, the concetration of Ce^{3+} cations is quantitatively evaluated by calculating the M_5/M_4 ratio via a second derivative method (see details in Figure S10).[38-39, 53] The average ratio calculated from serval NCs for each sample is poltted in blue ball Figure 4B. The M_5/M_4 ratio is 0.9954, 1.1530, 1.1281 for Sm-CeONC-1, Sm-CeONC-8, and Sm-CeONC-30, respectively. Therefore, the cubic CeO_2 NCs show the highest concentraton of Ce^{3+} of 60.74%, comparing to 21.34% in truncated octahedra and 54.52% in cuboctahedra by using the reference value of 1.31 for Ce^{3+}, and 0.91 for Ce^{4+}.[38-39, 54] Afterwards, the catalytic properties of as-synthesized Sm-CeONCs were evaluated by measuring the oxygen storage capacity (OSC) of the representative samples, as listed Table S2. The samples of Sm-CeONC exhibits superior OSC performance compared to the reference sample of CeO_2 commercial particles (2.5 μmol-O•g^{-1} at 400 °C, 25.6 μmol-O•g^{-1} at 500 °C). In detail, the OSC value is 183.3, 255.6, 319.5, 364.6, 355.5 μmol-O•g^{-1} at the test temperature of 400 °C for the samples of Sm-CeONC-1, -3, -6, -8 and 30, respectively. With the increased temperature to 500 °C, Sm-CeONC-1 shows the slightly increase to 252.2 μmol-O•g^{-1}, while the OSC values of Sm-CeONC-3, -6, -8 and -30 were much improved, displaying 455.6, 534.2, 620.1 and 638.0 μmol-O•g^{-1}, respectively. Such outstanding OSC performance of Sm-CeONCs is a quite improvement for the pristine CeO_2, even comparable to the other systems of doped CeO_2 nanocomposites in Table S3. Herein, the shape effct of Sm-CeONCs on the OSC performance is relatively reflected that it shows a gradual increase changing from Sm-CeONC-1 to Sm-CeONC-8, while subsequently a slightly decrease when the shape is Sm-CeONC-30, as illustrated by the bar graph in Figure 4B. The cubic NCs (Sm-CeONC-8) tends to form the stable and ordered constructions, which is supposed to maintain their structures after the removal of surfactant and the pre-heat process before OSC test. Thus, {100}-faceted cubic NCs are mostly preserved when testing at 400 °C, leading to a slightly larger OSC value of Sm-CeONC-8 (364.7 μmol-O•g^{-1}) than Sm-CeONC-30 (355.5 μmol-O•g^{-1}), which is attributed to the high concentration of Ce^{3+} of cubic NCs that mostly exposes the active {100} facets in 88.20% fraction. These results also manifest that there exists a competitive and complemental effect between the exposing facets and size on the OSC performance in the way that {100} active facets play an indispensable role on the OSC performance at a moderate test temperature (200-400 °C), whereas the effect of NCs size becomes dominated role at the test temperature of over 500 °C.[38, 55] Totally, it is witnessed the excellent OSC performance of the surfactant-modified cubic CeO_2 NCs, which is a great improvement for the CeO_2-based nanocatalysts in the industrial practical applications.

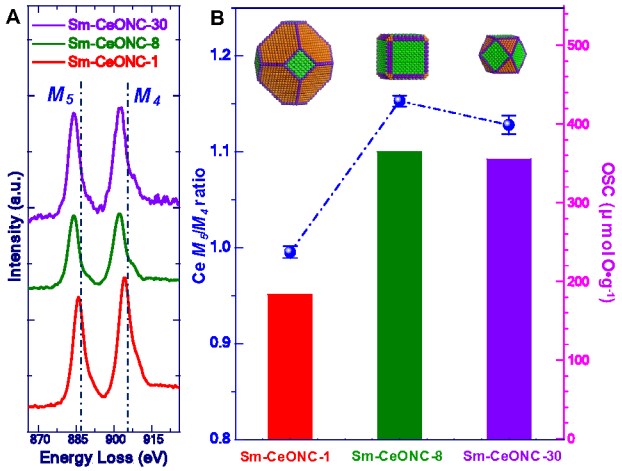

Figure 4. Shape-dependent of Ce valence state and Oxygen storage capacity (OSC) of the representative samples of Sm-CeONCs. (A) STEM-EELS Ce *M* edge spectra; (B) the corresponding M_5/M_4 ratio (blue plot) and OSC of at the temperature of 400°C. Dotted lines in (A) indicate the Ce M edge of bulk CeO_2.

The supercapatior properties of as-synthesized Sm-CeONCs were also evaluated by measuring the electrochemical performance of the representative samples, as depicted in Figure 5. It shows the cyclic voltammogram (CV) response of the representatively samples of Sm-CeONCs at the scan rate of 10 mV•s^{-1} in Figure 5A. For all the CV curves, a nonrectangular shape is clearly observed, which is attributed to the predominantly pseudocapacitance, and a pair of redox peaks corresponding to the oxidation and reduction of CeO_2 nanostructures ($Ce^{4+} \leftrightarrow Ce^{3+}$).[56] From the galvanostatic discharge profiles as plotted in Figure 5B, it is calculated that the electrode of Sm-CeONC-30 shows a high specific capacitance of 339.5 F•g^{-1}, compared to the other Sm-CeONCs electrodes of Sm-CeONC-8 (287.0 F•g^{-1}), Sm-CeONC-1 (186.5 F•g^{-1}) in 6 M KOH electrolyte at a current density of 1 A•g^{-1}. Figure 5C shows the specific capacitance of the Sm-CeONC electrodes as a function of applied current density. As can be seen, the specific capacitance shows a slight decrease with the increase of current density, which is attributed to the due to the reduced surface area accessed by the electrolyte at a high current density.[57] In particular, the gravimetric capacitance of Sm-CeONC-30 reaches 161.0 F•g^{-1} even at a current density of 20 A•g^{-1}, which is higher than those of the Sm-CeONC-8 (136.3 F•g^{-1}) and Sm-CeONC-1 (90.1 F•g^{-1}). The cycling performance of Sm-CeONCs electrodes were further evaluated at the current density of 10 A•g^{-1} for 1000 cycles (Figure 5D). The specific capacitance of these samples decreases with the cycle number, and the sample of Sm-CeONC-30 and Sm-CeONC-8 depicts a better cycling stability with a high specific capacitance after 1000 cycles. In addition, both of Sm-CeONC-30 and Sm-CeONC-8 electrodes possess relatively higher specific capacitance compared to previously reported CeO_2 NCs electrodes, and even comparable to some CeO_2-based nanomaterials electrodes, as summarized in Table S4. Moreover, it is shown in Figure S11 that for Sm-CeONC-8 and Sm-CeONC-30 electrodes, the pseudocapacitance still reaches 138 and 148 F•g^{-1} after 1000 cycles, which maintains approximately 92% and 84.09% of its initial capacitance, respectively. Comparatively, the electrodes of Sm-CeONC-8 present a larger specific capacity, better rate performance, and higher recycling stability, which are resulted from relatively high concentration of reduced cerium cations due to the exposure of highly reactive facets of {100} and smaller NCs size at the condition of appropriate surfactant addition. Lower surfactant-modified CeO_2 NCs would cause NCs aggregation, leading to the decreasing of redox active sites and increasing of internal resistance, which in total contributes toward the capacitance faded.[58]

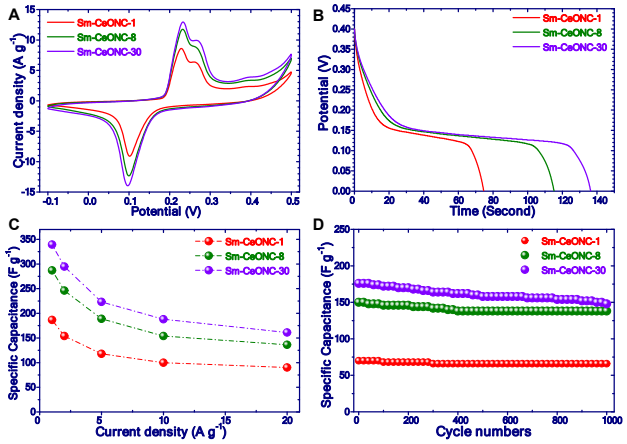

Figure 5. Supercapacitor performance of the representative electrodes of Sm-CeONCs in 6 M KOH. A) Cyclic voltammetry curves at the scan rate of 10 mV•s^{-1}, B) Galvanostatic discharge curves at the current density of 1 A•g^{-1}, C) Specific capacitance at different current density; D) Cycling performance at the current density of 10 A•g^{-1}.

Conclusions

In summary, with the aim of elucidating the mechanism of surfactant-mediated morphology evolution and self-assembly of CeO_2 nanocrystals, we have systematically synthesized a batch of surfactant modified CeO_2 NCs, and subsequently conducted the characterization by the means of aberration corrected STEM imaging and EELS techniques. It is found that the surfactant ligand plays a significant effect on the morphology, size and distribution of CeO_2 NCs in the way that its carboxylic group preferentially bonds onto the Ce-terminated {100} facets. In addition, we offered the substantiation proofs for the proposed growth mechanism of cubic CeO_2 NCs under the modification of surfactant. The cubic NCs superstructures is readily constructed in monolayer and/or multilayer via a self-assembly method and it is the interpenetration interaction among the surfactant molecules from the nearby cubic NCs that ensures the well-distributed {100} face-to-face arrangement and maintains their multilayer superstructures. Moreover, the cubic CeO_2 NCs shows the higher concentraton of Ce^{3+} of 60.74%, comparing to 54.52% in cuboctahedra, and 21.34% in truncated octahedra. The excellent superior catalytic and supercapacitor performances of {100} faceted CeO_2 NCs over other CeO_2-based nanostructures and nanocomposites, could be attributed to the high fraction (82.20%) of active facets of {100} exposure, smaller size, great superstructure stability under a temperature of 200~500°C. In principle, we have enriched the fundamental understanding for the surfactant-mediated mechanism of facet evolution and the self-assembly of CeO_2 NCs, which hold substantial promise in industrial applications by rational designing of CeO_2 based nanocatalysts, solid electrolytes and biomedicines.

Experimental Sections

Surfactant-modified CeO_2 NCs synthesis. A supercritical hydrothermal method was used to synthesize CeO_2 NCs in this work.[27, 38] Briefly, a fresh-made aqueous solution of cerium hydroxide was prepared by mixing cerium (III) nitrate hexahydrate (99.95%, Aladdin) and sodium hydroxide (98%, Aladdin). Then, 25 mL of the above precursor solution was placed in the pressure-resistant Hastelloy vessel (inner volume, 50 mL) with decanoic acid ($CH_3(CH_2)_8COOH$) as the organic surfactant. Next, the reaction occurred in a reactor at 180 °C for 20 min, subsequently into the reactor at 400 °C for 15 min. The surfactant addition was adjusted from 0:1 to 1:1, 2:1, 3:1, 5:1, 6:1, 8:1, 15:1, 30:1 (molar ratio to Ce in the precursor), to obtain the different modified NCs. After this, the surfactant-modified CeO_2 NCs were collected from the mixture, purified, and dried using a freezing drying procedure.

Characterization of surfactant-modified CeO_2 NCs. For electron microscopic characterization, one drop (10 μL) of the redispersed CeO_2 NCs solutions were directly deposited onto a carbon film (~5 nm). Low-magnification TEM images were taken using JEM-2100Plus (JEOL Co., Ltd.) with an accelerating voltage of 200 kV. Aberration-corrected STEM characterization was conducted by using a JEM-ARM 300F (Cold Field Emission Gun) with both probe and image correctors at the accelerating voltage of 300 kV. The convergence angle was ≈ 24.5 mrad, and the collection angle of the detector were 11-22 and 54–220 mrad, respectively. The EELS spectra were recorded using a Gatan Enfnium camera system with an energy spread ΔE of ≈ 0.3 eV.

Oxygen Storage Capacity of surfactant-modified CeO_2. The powder CeO_2 NCs products were heat-treated at 300 °C for 2 h to remove the organic surfactant.[59] The OSC property was measured by using a gas adsorption/desorption apparatus (Microtrac BEL, BELSORP CAT-II). About 50

mg of the powder sample of CeO_2 NCs was loaded and reduced sufficiently by hydrogen gas (99.999%) at the measurement temperature. Then the oxygen pulse (99.999%) was introduced and the decrease of the oxygen concentration was monitored with a thermal conductor detector (carrier gas: He, 99.999%). Finally, the oxygen storage amount was evaluated from the decrease of the O_2 pulse peak. As a reference, CeO_2 commercial powder (99.995%, Sigma-Aldrich) was also treated with the same procedure in the OSC test.

Supercapacitor performance of surfactant-modified CeO_2. The supercapacitor performance was conducted using a three-electrode analysis. Nickel foam was first pretreated successively with diluted hydrochloric acid and absolute ethanol to ensure a clean surface. The pure CeO_2 electrode were fabricated as follows: a mixture of hybrid powders containing 15 wt.% of acetylene black (as the electrical conductor), 5 wt.% of polytetrafluorene−ethylene (as the binder) as well as 80 wt.% of the samples, and small amount of ethanol was prepared by milling to produce homogeneous slurry. The mixture slurry was then pressed onto the foamed nickel (1 cm^2) electrode and dried at 110 °C for 8 h, and followed by pressing under a pressure of 5 MPa. The loading mass of active material was ~3 $mg•cm^{-2}$. All electrochemical measurements were carried out at room temperature in a 6 $mol•L^{-1}$ KOH aqueous electrolyte on a CHI 600E electrochemical workstation (ChenHua Instruments, Shanghai), The electrochemical properties of the products were investigated with cyclic voltammetry (CV), galvanostatic discharge/charge (GDC) tests and electrochemical impedance spectroscopy (EIS) which were obtained using an AC voltage of 5 mV in a frequency range from 0.01Hz to 100 kHz. The specific capacitances (C_s, $F•g^{-1}$) were calculated according to the following equations:

$$C_s = \frac{I\Delta t}{m\Delta V} \quad (1)$$

where I (mA) is the constant discharge current, Δt (s) is the discharging time, m (mg) is the total mass of active materials in both electrodes, ΔV (V) is the operation voltage window obtained from the discharge curve excluding the voltage drop.

Author Contributions

X. H. performed the nanocrystals synthesis and TEM/STEM observations, processed the experimental data and drafted the manuscript. S. Z., Y, X., L. T., and S. M. helped to nanocrystals synthesis and properties tests. K. I., M. S., and C. C., supported the microscopic experiments and data analysis. B. X., T. A., and Y. I directed the entire study. All authors participated in discussions and commented on the manuscript.

Conflicts of interest

There are no conflicts to declare.

Acknowledgements

X. H. gratefully acknowledges the financial support from National Natural Science Foundation of China (Grant Number 21902096); Natural Science Foundation of Shaanxi Province (Grant Number 2020JQ-709); the Natural Science Special Project of Education Department of Shaanxi Province (Grant Number 19JK0136); the Open Foundation of The New Style Think Tank of Shaanxi Universities (Research Center for Auxiliary Chemistry and New Materials Development, Shaanxi University of Science and Technology, ACNM-202006); and Scientific Research Foundation of Shaanxi University of Science and Technology. A.T. thanks for the support from Japan Science and Technology Agency (JST) [MIRAI, Grant Number JPMJMI17E4 and CREST, Grant Number JPMJCR16P3]; the New Energy and Industrial Technology Development Organization of Japan (NEDO); JSPS KAKENHI (Grant Number JP16H06367 and JP20K20548); Materials Processing Science Project (Materealize; Grant Number JPMXP0219192801) of the Ministry of Education, Culture, Sports, Science and Technology (MEXT), and World Premier International Research Center Initiative (WPI), MEXT, Japan. Y. I. is thankful for the support from Grant-in-Aid for Specially Promoted Research (Grant Number 17H06094) from Japan Society for the Promotion of Science and "Nanotechnology Platform" (Grant Number JPMXP09A17UT0232) from MEXT.

Notes and references

[1] Wang, X., Zhuang, J., Peng, Q., Li, Y., *Nature*, 2005, **437**, 121.
[2] Wang, Z. L., *J. Phys. Chem. B*, 2000, **104**, 1153.
[3] Burda, C., Chen, X., Narayanan, R., El-Sayed, M. A., *Chem. Rev.*, 2005, **105**, 1025.
[4] Talapin, D. V., Lee, J. S., Kovalenko, M. V., Shevchenko, E. V., *Chem. Rev.*, 2010, **110**, 389.
[5] Yuan, M., Guo, X., Li, N., Pang, H., *Journal of Colloid and Interface Science*, 2021, **589**, 56.
[6] Chen, T., Bai, Y., Xiao, X., Pang, H., *Chem. Eng. J.*, 2020, 127523.
[7] Xue, Y., Hang, X., Ding, J., Li, B., Zhu, R., Pang, H., Xu, Q., *Coordin. Chem. Rev.*, 2020, 213656.
[8] Li, X., Yang, X., Xue, H., Pang, H., Xu, Q., *EnergyChem*, 2020, **2**, 100027.
[9] Guo, Z., You, Q., Song, L., Sun, G., Chen, G., Li, C., Yang, X., Hu, X., Jiang, X., *Nanoscale*, 2021, **13**, 117.
[10] Park, J., An, K., Hwang, Y., Park, J. G., Noh, H. J., Kim, J. Y., Park, J. H., Hwang, N. M., Hyeon, T., *Nat. Mater.*, 2004, **3**, 891.
[11] Min, Y., Akbulut, M., Kristiansen, K., Golan, Y., Israelachvili, J., *Nat. Mater.*, 2008, **7**, 527.
[12] Murray, C. B., Kagan, C. R., Bawendi, M. G., *Science*, 1995, **270**, 1335.
[13] Talapin, D. V., Shevchenko, E. V., Kornowski, A., Gaponik, N., Haase, M., Rogach, A. L., Weller, H., *Adv. Mater.*, 2001, **13**, 1868.
[14] Bigioni, T. P., Lin, X. M., Nguyen, T. T., Corwin, E. I., Witten, T. A., Jaeger, H. M., *Nat. Mater.*, 2006, **5**, 265.
[15] Dong, A., Chen, J., Vora, P. M., Kikkawa, J. M., Murray, C. B., *Nature*, 2010, **466**, 474.
[16] Sun, S., Murray, C. B., Weller, D., Folks, L., Moser, A., *Science*, 2000, **287**, 1989.
[17] Bao, J., Bawendi, M. G., *Nature*, 2015, **523**, 67.
[18] Boles, M. A., Engel, M., Talapin, D. V., *Chem. Rev.*, 2016, **116**, 11220.
[19] Zherebetskyy, D., Scheele, M., Zhang, Y., Bronstein, N., Thompson, C., Britt, D., Salmeron, M., Alivisatos, P., Wang, L. W., *Science*, 2014, **344**, 1380.
[20] Boles, M. A., Ling, D., Hyeon, T., Talapin, D. V., *Nat. Mater.*, 2016, **15**, 141.
[21] Jun, Y., Casula, M. F., Sim, J. H., Kim, S. Y., Cheon, J., Alivisatos, A. P., *J. Am. Chem. Soc.*, 2003, **125**, 15981.
[22] Tao, A. R., Habas, S., Yang, P., *Small*, 2008, **4**, 310.
[23] Ong, Q., Luo, Z., Stellacci, F., *Acc. Chem. Res.*, 2017, **50**, 1911.
[24] Mancini, G. F., Latychevskaia, T., Pennacchio, F., Reguera, J., Stellacci, F., Carbone, F., *Nano Lett.*, 2016, **16**, 2705.
[25] Zhang, H., Chi, L., *Adv. Mater.*, 2016, **28**, 10492.
[26] Simon, P., Bahrig, L., Baburin, I. A., Formanek, P., Roder, F., Sickmann, J., Hickey, S. G., Eychmuller, A., Lichte, H., Kniep, R., Rosseeva, E., *Adv. Mater.*, 2014, **26**, 3042.
[27] Hao, X., Chen, C., Saito, M., Yin, D., Inoue, K., Takami, S., Adschiri, T., Ikuhara, Y., *Small*, 2018, **14**, 1801093.
[28] Liao, H. G., Zherebetskyy, D., Xin, H., Czarnik, C., Ercius, P., Elmlund, H., Pan, M., Wang, L. W., Zheng, H., *Science*, 2014, **345**, 916.
[29] Hauwiller, M. R., Frechette, L. B., Jones, M. R., Ondry, J. C., Rotskoff, G. M., Geissler, P., Alivisatos, A. P., *Nano Lett.*, 2018, **18**, 5731.
[30] Hens, Z., De Roo, J., *J. Am. Chem. Soc.*, 2020, **142**, 15627.
[31] Trovarelli, A., *Catal. Rev.*, 1996, **38**, 439.
[32] Chueh, W. C., Falter, C., Abbott, M., Scipio, D., Furler, P., Haile, S. M., Steinfeld, A., *Science*, 2010, **330**, 1797.
[33] Paier, J., Penschke, C., Sauer, J., *Chem. Rev.*, 2013, **113**, 3949.
[34] Lee, J. G., Park, J. H., Shul, Y. G., *Nat. Commum.*, 2014, **5**, 4045.

[35] Wang, M., Shen, M., Jin, X., Tian, J., Zhou, Y., Shao, Y., Zhang, L., Li, Y., Shi, J., *Nanoscale*, 2020, **12**, 12374.
[36] Cordeiro, M. A. L., Weng, W., Stroppa, D. G., Kiely, C. J., Leite, E. R., *Chem. Mater.*, 2013, **25**, 2028.
[37] Zhang, J., Ohara, S., Umetsu, M., Naka, T., Hatakeyama, Y., Adschiri, T., *Adv. Mater.*, 2007, **19**, 203.
[38] Hao, X., Yoko, A., Chen, C., Inoue, K., Saito, M., Seong, G., Takami, S., Adschiri, T., Ikuhara, Y., *Small*, 2018, **14**, 1802915.
[39] Hao, X., Yoko, A., Inoue, K., Xu, Y., Saito, M., Chen, C., Seong, G., Tomai, T., Takami, S., Shluger, A. L., Xu, B., Adschiri, T., Ikuhara, Y., *Acta Mater.*, 2021, **203**, 116473.
[40] Trovarelli, A., Llorca, J., *ACS Catal.*, 2017, **7**, 4716.
[41] Tan, Z., Zhang, J., Chen, Y.-C., Chou, J.-P., Peng, Y.-K., *J. Phys. Chem. Lett.*, 2020, **11**, 5390.
[42] Tan, Z., Li, G., Chou, H.-L., Li, Y., Yi, X., Mahadi, A. H., Zheng, A., Edman Tsang, S. C., Peng, Y.-K., *ACS Catal.*, 2020, **10**, 4003.
[43] Taguchi, M., Takami, S., Naka, T., Adschiri, T., *Cryst. Growth Des.*, 2009, **9**, 5297.
[44] Coropceanu, I., Boles, M. A., Talapin, D. V., *J. Am. Chem. Soc.*, 2019, **141**, 5728.
[45] Ye, X., Chen, J., Eric Irrgang, M., Engel, M., Dong, A., Glotzer, Sharon C., Murray, C. B., *Nat. Mater.*, 2016, **16**, 214.
[46] Yu, C., Guo, X., Muzzio, M., Seto, C. T., Sun, S., *Chemphyschem*, 2019, **20**, 23.
[47] Findlay, S. D., Shibata, N., Sawada, H., Okunishi, E., Kondo, Y., Yamamoto, T., Ikuhara, Y., *Appl. Phys. Lett.*, 2009, **95**, 191913.
[48] Findlay, S. D., Shibata, N., Sawada, H., Okunishi, E., Kondo, Y., Ikuhara, Y., *Ultramicroscopy*, 2010, **110**, 903.
[49] Boneschanscher, M. P., Evers, W. H., Geuchies, J. J., Altantzis, T., Goris, B., Rabouw, F. T., Van Rossum, S., van der Zant, H. S., Siebbeles, L. D., Van Tendeloo, G., *Science*, 2014, **344**, 1377.
[50] Litwinowicz, A.-A., Takami, S., Asahina, S., Hao, X., Yoko, A., Seong, G., Tomai, T., Adschiri, T., *CrystEngComm*, 2019, **21**, 3836.
[51] Wu, L., Willis, J. J., McKay, I. S., Diroll, B. T., Qin, J., Cargnello, M., Tassone, C. J., *Nature*, 2017, **548**, 197.
[52] Zhu, M., Wen, Y., Song, S., Zheng, A., Li, J., Sun, W., Dai, Y., Yin, K., Sun, L., *Nanoscale*, 2020, **12**, 19104.
[53] Fortner, J. A., Buck, E. C., *Appl. Phys. Lett.*, 1996, **68**, 3817.
[54] Wu, L., Wiesmann, H. J., Moodenbaugh, A. R., Klie, R. F., Zhu, Y., Welch, D. O., Suenaga, M., *Phys. Rev. B*, 2004, **69**, 125415.
[55] Zhang, J., Kumagai, H., Yamamura, K., Ohara, S., Takami, S., Morikawa, A., Shinjoh, H., Kaneko, K., Adschiri, T., Suda, A., *Nano Lett.*, 2011, **11**, 361.
[56] Maiti, S., Pramanik, A., Mahanty, S., *Chem. Comm.*, 2014, **50**, 11717.
[57] Zhu, S. J., Jia, J. Q., Wang, T., Zhao, D., Yang, J., Dong, F., Shang, Z. G., Zhang, Y. X., *Chem. Comm.*, 2015, **51**, 14840.
[58] Jeyaranjan, A., Sakthivel, T. S., Molinari, M., Sayle, D. C., Seal, S., *Part. Part. Syst. Char.*, 2018, **35**, 1800176.
[59] Li, D., Wang, C., Tripkovic, D., Sun, S., Markovic, N. M., Stamenkovic, V. R., *ACS Catal.*, 2012, **2**, 1358.